CryoEM structures of the multimeric secreted NS1, a major factor for dengue hemorrhagic fever

Authors: Bo Shu, Justin S.G. Ooi, Aaron W.K Tan, Thiam-Seng Ng, Wanwisa Dejnirattisai, Juthathip Mongkolsapaya, Guntur Fibriansah, Jian Shi, Victor A. Kostyuchenko, Gavin Screaton, Shee-Mei Lok*

*Correspondence: Shee-Mei Lok (sheemei.lok@duke-nus.edu.sg)

Abstract

Dengue virus infection can cause dengue hemorrhagic fever (DHF). Dengue NS1 is multifunctional: the intracellular dimeric NS1 (iNS1) forms part of the viral replication complex, the extracellular multi-oligomeric secreted NS1 (sNS1) is a major factor contributing to DHF. The structure of the iNS1 is well studied but not sNS1. Here we show the tetrameric (stable and loose conformation) and hexameric structures of sNS1. Stability of the stable and loose tetramers is determined by the conformation of their N-terminal domain – elongated β-sheet or β-roll. Binding of an anti-NS1 Fab breaks the loose tetrameric and hexameric sNS1 into dimers, whereas the stable tetramer remains largely unbound. Our results show detailed quaternary organization of different oligomeric states of sNS1 and will contribute towards the design of dengue therapeutics.

Main

Dengue is a positive sense single-stranded RNA enveloped virus. It belongs to the family *Flaviviridae*, which also includes significant human pathogens like West Nile (WNV), yellow fever (YF) and Zika virus (ZIKV). Dengue virus causes disease that ranges from mild dengue fever to the severe dengue hemorrhagic fever (DHF) and the dengue shock syndrome (DSS)[1]. There are four DENV serotypes. Dengvaxia, which is currently the only licensed dengue vaccine, has an overall efficacy of only 45%, and there is a possibility of priming the previously immune naïve children to develop severe disease in subsequent natural infection after vaccination [2]. It has proven to be difficult to develop an effective vaccine using whole dengue virus or its surface E protein, as the vaccine would need to stimulate equally strong immune responses simultaneously against all four dengue serotypes or else it can lead to a possibility of antibody-dependent enhancement (ADE) of infection[3]. This could lead to severe DHF/DSS.

Recently, dengue non-structural protein 1 (NS1) has been investigated as an alternative protein candidate for vaccine development. It has been shown to play an important role in causing the vascular leakage symptoms in DHF/DSS[4]. NS1 is secreted alongside dengue virus particles during an infection. It is a multifunctional protein which exists in different oligomeric forms intracellularly and extracellularly[5], and they play distinctly different roles. The intracellular NS1 (iNS1), exists as membrane associated dimeric form and is a part of the viral replication complex. The extracellular secreted NS1 (sNS1), exists in higher oligomeric forms. sNS1 likely causes vascular leakage symptoms in DHF/DSS via two pathways – indirectly, by stimulating the innate immune response through activation of complement and Toll-like receptors[6], and directly, by binding to endothelial cells causing endothelial hyperpermeability. sNS1 when bound directly to endothelial cells causes barrier dysfunction of the cell monolayer as demonstrated in an *in vitro* trans-

38 endothelial electrical resistance (TEER) assay[4,7]. *In vivo* studies show that the sNS1 is present
39 at very high concentrations in patient sera and correlates closely with the severity of disease [8].
40 Mice injected with sNS1 along with a sublethal dose of DENV were observed to succumb to
41 infection. Injection of sNS1 alone also causes vascular leakage in mice[4]. NS1-immune
42 polyclonal serum and anti-NS1 monoclonal antibodies (MAbs) can protect mice against
43 lethal DENV2 challenge [4]. sNS1 was also found to enhance viral infection in mosquitoes by
44 downregulating mosquito midgut immune genes[9]. sNS1 is therefore an important viral
45 protein both for viral infection (mammalian cells and mosquitoes) and pathogenesis, and it is
46 important to understand the structure of the sNS1 protein.

47 iNS1 (45 kDa) is first made in the endoplasmic reticulum (ER) as a monomer. It then
48 forms dimers and is glycosylated in the ER and the trans-Golgi network. It is eventually
49 transported to the cell membrane where some is secreted outside the cell, becoming sNS1.
50 There is a high-resolution crystal structure of full length dimeric dengue iNS1[10] produced by
51 baculovirus expression and subsequent extraction from cellular membrane compartments .
52 There are also crystal structures of the dimeric form of NS1 protein from other flaviviruses[11]
53 and they are largely similar to that of the DENV iNS1. Each protomer of the iNS1 contains
54 three domains (Extended data Fig. 1A): 1) the N-terminus contains the β-roll domain (amino
55 acids 1-30) that interacts with the same domain from the other protomer within the dimer to
56 form a roll-like structure (named β-roll). This domain is generally hydrophobic and is thought
57 to interact with cellular membranes. 2) Following the β-roll domain is the wing domain
58 (amino acids 31-181). The wing domain is the most flexible domain as it differs between
59 different flavivirus NS1 crystal structures [11]. 3) the β-ladder domain (amino acids 182-352),
60 consists of a continuous arrangement of 10 β-strands. The β-ladder domains from the two
61 iNS1 protomers line up with each other to form a long ladder-like pattern. One side of the β-
62 ladder faces the hydrophobic β-roll, while the other side is decorated with its highly charged

63 spaghetti loops. The interaction between protomers within the dimer is stabilized by a large
64 number of hydrogen bonds[12].

65 About a decade ago, two very low resolution (23 Å and 30 Å) EM structures of sNS1
66 were determined: a cryoEM structure reconstructed from images acquired by using an 120kV
67 LaB_6-equipped electron microscope (Philip CM12 TEM)[13] and the other, a negative stained
68 room temperature EM structure (Extended data Fig. 1B)[14]. Both maps had an overall hollow
69 barrel-like structure lacking fine structural details. Since then, the availability of 300kV
70 transmission electron microscopes equipped with direct electron detectors and field emission
71 gun electron sources, as well as improved cryoEM reconstruction methods, have made more
72 routine determination of cryoEM structures of small proteins to high resolution possible.
73 Here we report the cryoEM structures of sNS1 tetramers (dimer of dimers) and hexamers
74 (trimer of dimers) from a DENV2 clinical strain PVP94/07. We observe sNS1 exists
75 predominantly in the tetrameric form. There are two tetrameric states - stable and loose, and
76 some of these structures are determined to ~3.5Å resolution. The most obvious and dramatic
77 difference between the stable and loose tetramers is the organization of their N-terminal
78 domains – elongated β-sheet and β-roll, respectively. Only a minority of the sNS1 population
79 is hexameric and this cryoEM structure was determined to 8Å resolution. We also determined
80 a structure of sNS1 complexed with a Fab 5E3 to 3.5Å resolution. Most of the sNS1 (loose
81 tetramers and hexamers) dissociates into dimers when bound to Fab, while the stable tetramer
82 remains largely unbound. This is consistent with our results showing the ability of the Fab
83 5E3 to only partially inhibit sNS1-induced endothelial cell permeability. This study shows
84 sNS1 exists in a heterogenous mixture of oligomerization states, and we present the first high
85 resolution structures of sNS1.

86

87 **sNS1 from DENV2 contains heterogenous oligomeric states with tetramers as the**
88 **predominant population.**

89 His-tagged NS1 (DENV2 clinical strain PVP94/07) was expressed in human
90 embryonic kidney (HEK) cells. We harvested the sNS1 from tissue culture supernatant and
91 after purification, we analyzed it using coomassie blue stained semi-denaturing SDS-PAGE
92 gel (the sample was not boiled nor exposed to DTT). The gel shows clear bands
93 corresponding to dimers and tetramers (Fig. 1A). As the sample was exposed to SDS, a
94 detergent, the presence of tetramer band suggests that the tetramer is resistant to detergent.
95 We then performed cross-linking of sNS1 with bis(sulfosuccinimidyl) suberate (BS^3) before
96 analyzing it by denaturing SDS-PAGE. This showed the presence of aggregates, which could
97 be due to BS^3 non-specifically crosslinking proteins, as well as bands for hexamer, tetramer,
98 dimer and monomer (Fig. 1B). These results also showed that the tetrameric form is the
99 predominant oligomerization state in the NS1 protein sample.

100 We collected 7714 cryoEM micrographs (Table S1) and observed particles with
101 distinct shapes (Fig. 1C). We then performed several cycles of 2D classification and
102 alignment of the boxed particles. The 2D class averages show particles with different features
103 (Fig. 1D) - some appearing like stable and loose tetramers and others like hexamers. We did
104 not observe any sNS1 dimers. This suggests that sNS1 consists of heterogenous populations
105 of particles with likely tetrameric and hexameric states.

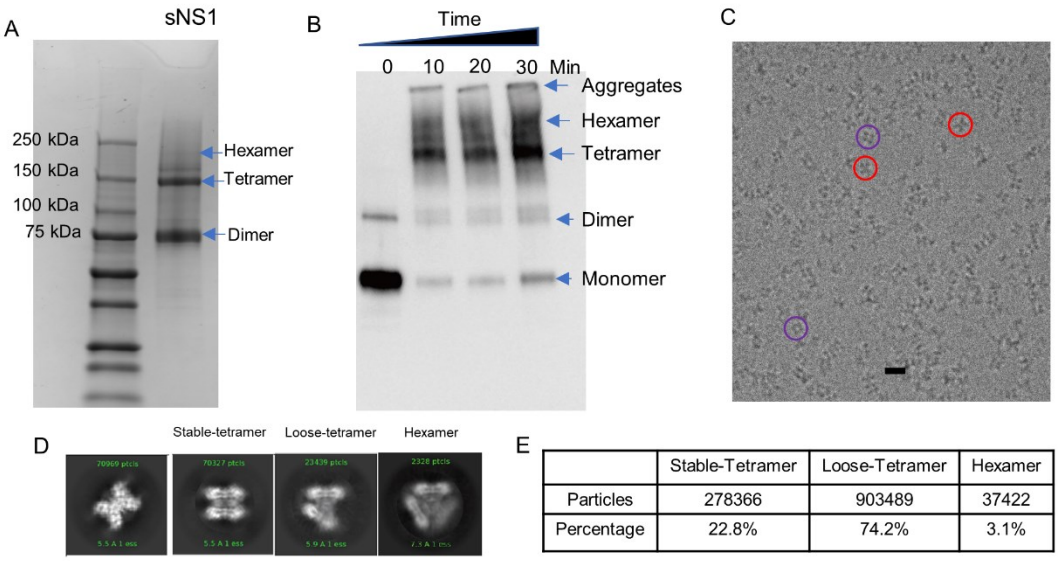

	Stable-Tetramer	Loose-Tetramer	Hexamer
Particles	278366	903489	37422
Percentage	22.8%	74.2%	3.1%

Fig. 1 Profile of the sNS1 from DENV2 (PVP94/07) clinical strain. **(A)** Semi-denaturing SDS-PAGE gel (non-boiling and no DTT) shows the clear dimer and tetramer bands, along with a very faint hexamer band. **(B)** Western blot denaturing SDS-PAGE gel (using Anti-polyHistidine–Peroxidase antibody) analysis of sNS1 cross-linked with BS^3 at different incubation times. Aggregates, hexamers, tetramers, dimers and monomers were seen. **(C)** A cryoEM micrograph of the sNS1 showing distinct-shaped particles, e.g., butterfly-shaped (red circles) and cube-shaped particles (purple circles). Scale bar is 10 nm. **(D)** The 2D class averages indicate that the particles are heterogenous, with some likely existing as tetramers (stable and loose forms) and others as hexamers. **(E)** The distribution of particles in different oligomerization states determined after 3D classification and refinement. Most of the particles are tetramers (loose and stable) and hexamers are a minority in the population.

119 **CryoEM reconstruction of different oligomeric states of sNS1**

120 As sNS1 consists of a heterogenous population of particles of different
121 oligomerization states, we performed a 3D classification using the program Relion [15]
122 (Extended data Fig. 2). The first round of unsupervised classification was done assuming no
123 symmetry (C1) to avoid bias towards any specific oligomerization states. We then performed
124 rough fitting with a dimeric NS1 crystal structure into these maps to determine their
125 oligomerization states (Extended data Fig. 3). We observed two maps that correspond to
126 tetramers: one with clear densities suggesting that the overall structure is quite stable
127 (Extended data Figs. 2-3), while the other with looser interactions between the two dimers
128 and poorer map resolution (Extended data Fig. 2). We refer the former as stable tetramer and
129 the latter, as loose tetramer. We also observed a 3D class that is hexameric in structure
130 (Extended data Figs. 2-3). Consistent with the 2D class averages, the 3D classification also
131 did not yield any dimeric structures. We then used the maps from 3D classification in Relion
132 as initial models for further classification and refinement in the program CryoSPARC [16]. For
133 the stable tetramers, we performed multiple cycles of heterogenous and non-uniform
134 refinement [17] by imposing D2 symmetry and obtained a final map of 3.5Å resolution (Fig. 2A
135 and Extended data Fig. 4), as measured by gold standard FSC curve cutoff at 0.143. For the
136 loose tetramers, we performed heterogenous and non-uniform refinement with no symmetry
137 imposed, and we determined one subclass of the loose tetramer to 8 Å resolution (Fig. 3A(i)
138 and Extended data Fig. 5A). We then performed local refinement on one of its dimers and
139 obtained a 3.4 Å cryoEM density map (Fig. 3A(ii) and Extended data Fig. 5B). For the
140 hexamers, since we only had a limited number of particles (~30,000 particles), we performed
141 only non-uniform refinement with D3 symmetry imposed and obtained an 8Å map (Figs. 3B
142 and Extended data Fig.6). The cryoEM reconstruction flow chart is summarized in Extended
143 data Fig. 2 and validation statistics in Extended data Table 1.

144 **Structure of sNS1 stable tetramers**

145 The 3.5Å resolution sNS1 stable tetramer cryoEM map shows clear separation
146 between β-strands (Extended data Figs. 4C-D). We also calculated the local resolution
147 (Extended data Fig. 4A) of the map. While most of the density map is ~3.5 Å resolution,
148 parts of the map (corresponding to the β-ladder) are at ~3.0Å resolution with some of the side
149 chain densities resolved (Extended data Fig. 4D). The resolution of the wing domain and the
150 β-roll was lower (4.0 to 4.5 Å). The density of both N- (residues 1-11) and C- terminal ends
151 (residues 341-352) is missing from the map.

152 We interpreted the stable tetramer (dimer of dimers) cryo-EM density by fitting in the
153 zika dimeric NS1 crystal structure (PDB:5GS6), because the structure is more complete than
154 the dengue iNS1, and then mutated it into dengue NS1 sequence (Figs. 2A-B and Extended
155 data Fig.4B). After fitting, we compared one of our sNS1 dimer in the stable tetramer to the
156 dengue iNS1 dimer (PDB:4O6B) and it shows the wing domain of our sNS1 dimer is rotated
157 by 6.8° with respect to the β-ladder. The β-roll structures of the two dengue iNS1 dimers
158 cannot fit well into the cryoEM density of the stable tetramer and they clash with each other.
159 Indeed, the space (25Å) between two dimers within the stable tetramers is not big enough to
160 accommodate the two iNS1 β-rolls. We observed that the β-roll densities, instead of
161 concentrating at the middle of the dimers as observed in iNS1 (Extended data Fig. 1), have an
162 elongated shape that stretches across the two protomers within a dimer (Figs. 2A and B). This
163 suggests that they have very different tertiary structures. Fitting of the density map shows that
164 residues 15 to 24 form a long β-strand which pairs with the same β-strand of the other
165 protomer within the dimer to form a long anti-parallel β-sheet (hereafter, referred to as
166 elongated β-sheet) (Figs 2A-B). As the resolution of this region is ~4.5 Å, we analyzed their
167 interaction by using a distance cut off of 8 Å between the Cα backbone. Using this criterion,
168 we observed that this elongated β-sheet from one dimer likely interacts with the same β-sheet

169 from the opposite dimer via electrostatic interactions or hydrogen bonds at both ends of each
170 respective β-sheet (Fig. 2C(i)-(ii)). Charge analysis in UCSF Chimera [18] shows that these
171 two ends have high charge complementarity between dimers (Fig. 2C (iii)), suggesting
172 possible hydrogen bonds or electrostatic interactions. Hydrophobic analysis shows that these
173 β-sheets have an overall highly hydrophobic surface that also plays an important role in
174 stabilizing their interactions.

175 We next compared the β-roll domain of iNS1 with the elongated β-sheet of the sNS1
176 stable tetramer. The iNS1 β-roll domain contains three β-strands (residues 1-7, 12-16 and 18-
177 22), whereas we were unable to observe any density for residues 1-11 in the sNS1 stable
178 tetramer, probably due to disorder in this region, and residues 15-24 form a long, continuous
179 β-strand. This raises a question: is the sNS1 tetramer assembled from dimers of iNS1? If so,
180 is it possible for the iNS1 β-roll structure to rearrange into the elongated β-sheet seen in the
181 stable tetramer? If this were to happen, it would require the second β-strand of iNS1 to rotate
182 by ~120° with respect to the third β-strand to form the long, continuous β-strand we observed
183 (Fig. 2D). Whether the iNS1 dimer is a precursor of the sNS1 stable tetramer is unknown. It
184 is also possible that the sNS1 stable tetramer is assembled during translation of the NS1
185 protein by a pathway independent of iNS1 dimer formation, before being secreted.

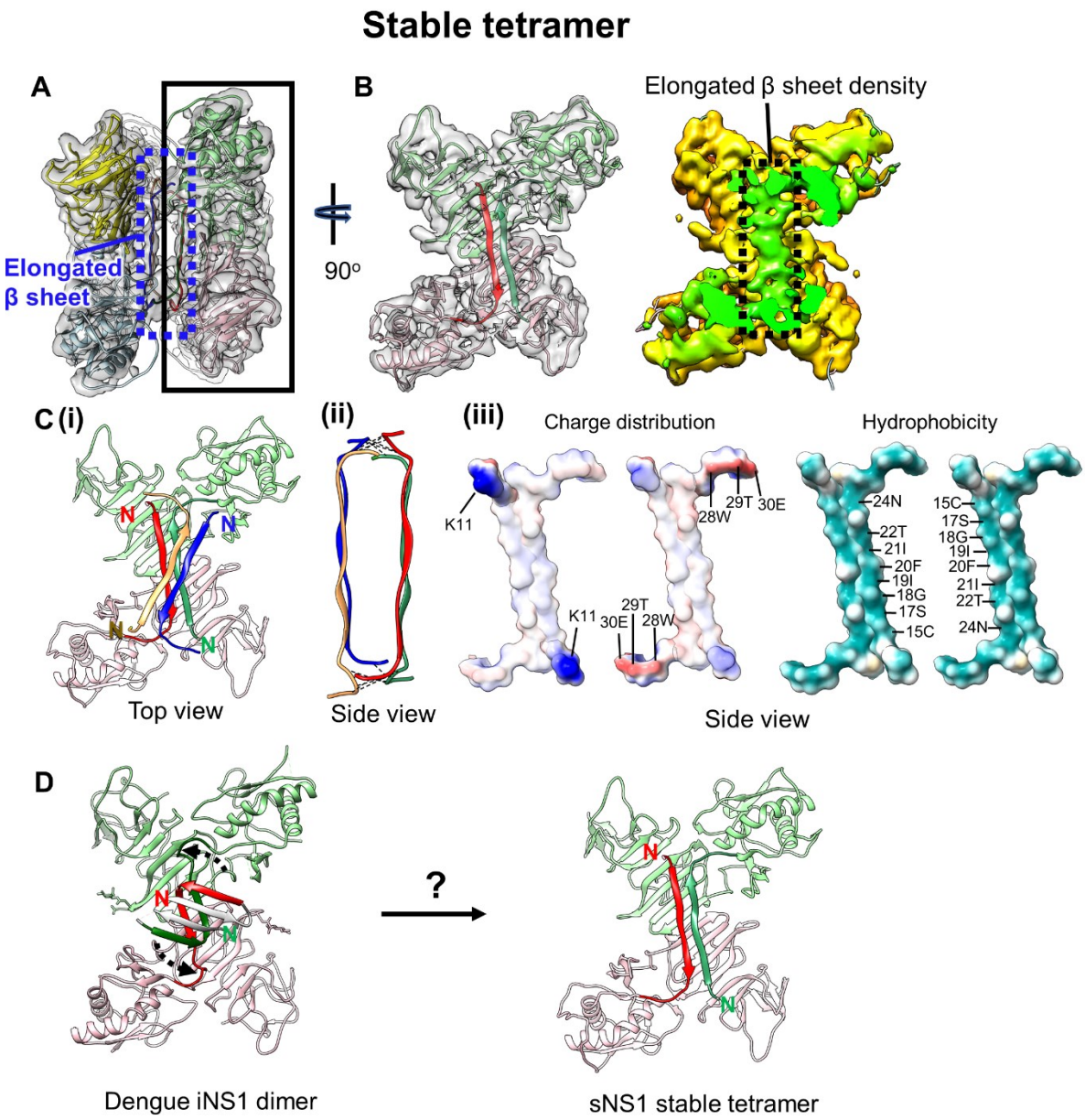

Fig. 2 Structure of the stable sNS1 tetramer. (**A**) Two NS1 dimeric structures fitted into the cryoEM map (reduced sharpening was applied to make the density of the elongated β-sheet clearer). One dimer is colored in pink and light green and the other in yellow and light blue. (**B**) Left: the overall structure of the sNS1 dimer is similar to that of iNS1 except for the β-roll region (residues 1-30) in iNS1, which is an elongated β-sheet (residues 15-24) in sNS1. View from the elongated β-sheet of the black boxed region in (A). The respective elongated β-strand of each protomer is highlighted in a darker shade of the same color (red and dark green). Right: surface density map with the regions corresponding to the elongated β-sheet colored in green, and the rest of the map in yellow. (**C**) Interaction of the elongated β-strands between the two dimers (red/green and yellow/blue). (i) Top view showing the elongated β-sheets of the red/green dimer interacting with that of the yellow/blue dimer (only its elongated β-sheet is shown). (ii) Side view showing possible hydrogen bonds or electrostatic interactions between the two elongated β-sheets from opposite dimers (dotted black lines).

These interactions are identified by the distance between Cα backbone (< 8Å) and also their charge characteristics. (iii) The interacting residues are complementary in both charges and hydrophobicity. Open book representation of (ii): (Left) charge, and (Right) hydrophobicity distributions on the surface of the two elongated β-sheets. For charge, positive charges are colored in blue while negative charges are red. For hydrophobicity, cyan color indicates hydrophobic residues. Possible interacting residues are labelled. **(D)** Comparison of iNS1 β-roll with sNS1 stable tetramer elongated β sheet and how it might change from the β-roll structure (dotted arrow on the iNS1 structure) into the elongated β sheet structure.

210

211 **CryoEM structure of loose sNS1 tetramers**

212 We also determined an 8Å resolution loose sNS1 tetramer structure (Figs. 3A(i) and
213 Extended data Fig.5A) and by focused refinement on one of its constituent dimers, we
214 obtained a 3.4Å resolution cryoEM map (Figs. 3A (ii) and Extended data Fig.5B (i-ii)). The
215 overall structure of the dimer and its β-roll (Fig. 3A (ii)) is very similar to that of iNS1
216 (RMSD 0.8 Å), unlike the stable sNS1 tetramer. The overall 8Å resolution loose sNS1
217 tetramer structure shows that the two dimers are rotated by ~35° with respect to each other
218 and extra density is visible between the β-rolls of these two dimers (Fig. 3A(i)). Our high
219 resolution sNS1 dimer structure within the loose tetramer also shows some strong extra
220 densities above the β-roll (Fig. 3A(iii)). Previous work from other research groups [13,14] show
221 that there are lipids associated with sNS1 that may help stabilize the overall structure, and
222 which may contribute to these uninterpreted densities.

223 The difference between the stable and the loose tetramers is whether the residues near
224 the N-terminus form a β-roll or an elongated β-sheet. Hence, this could be the determinant
225 that defines stability.

226 An existing crystal structure of a ZIKV sNS1 [11] (PDB code: 5GS6), obtained by
227 purifying sNS1 produced using a baculovirus expression system, is a dimeric structure.
228 However, upon examination of the crystal packing in this structure, sNS1 appears to have a
229 tetrameric structure similar to our loose tetramer (RMSD 4.2 Å) (Fig. 3A(iv)). This may
230 suggest that at least one of the ZIKV sNS1 oligomers might be the loose tetramer structure.

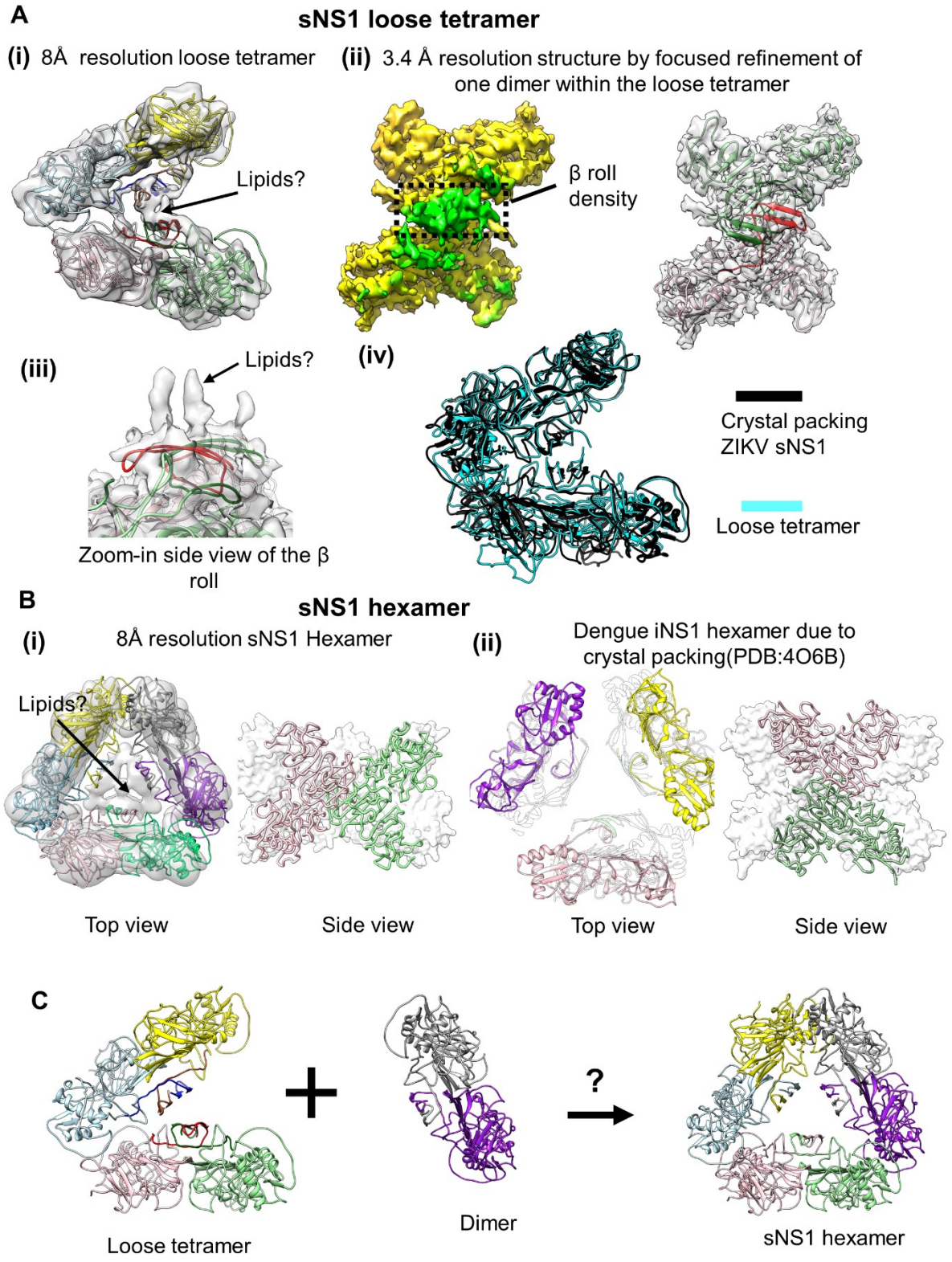

Fig. 3 CryoEM structures of the sNS1 loose tetramer and hexamer. **(A)** (i) The fit of sNS1 into the 8 Å resolution loose tetramer density map. (ii) Focused refinement of one dimer of the loose tetramer yields a 3.4Å resolution map. An iNS1 dimer fits well into the density showing that the loose tetramer contains a β-roll structure similar to that of iNS1. Left: cryoEM map with the density corresponding to the β-roll colored in green and the rest in

yellow. Right: the fit of the red/green dimer into the density. (iii) Zoom-in side view of the β-roll density (from (ii)) showing uninterpreted density that might belong to lipid molecules. (iv) Superposition of our loose tetramer with the tetramer observed in the crystal packing of ZIKV sNS1 structure (PDB: 5GS6) shows that they have similar structures. **(B)** Comparison of our sNS1 hexamer with the dengue iNS1 hexamer from the crystal packing. (i) Top and side views of the 8Å resolution sNS1 hexamer structure. Left: fit of three dimers into the cryoEM map. We are unable to discern whether sNS1 adopts a β-roll or an elongated β-sheet structure, as the interior of the hexamer contains unfeatured density. It may also contain lipid cargo as suggested by Gutsche and colleagues [14] (ii) The previously published dengue iNS1 structure [10] shows hexamers due to crystal packing; however, there is little interaction between the iNS1 dimers (left; top view). The dimers in the hexamer (right; side view) are also oriented differently to our hexameric structure (in (i), side view). **(C)** Interaction of a loose tetramer with a dimer could lead to the formation of a hexamer.

251 **CryoEM structure of the sNS1 hexamer**

252 We obtained an 8Å resolution sNS1 hexamer map (Figs. 3B(i) and S6A-B). The low
253 resolution structure suggests that the NS1 molecules in the hexameric state are interacting
254 loosely with each other. Fitting of iNS1 (Extended data Fig. 6C) suggests that three dimers
255 interact with each other via their wing domain and the distal end of the β-ladder. This
256 interaction is similar to that in the loose tetramer. The density in the central core of the
257 hexamer is weak (Extended data Fig. 6B) and we were therefore unable to determine if the
258 dimers have a β-roll or elongated β-sheet conformation. It is also possible that the interior of
259 this hexamer contains lipid cargo, as suggested by other research groups [13,14] and this may
260 prevent determination of the structure of this region.

261 The crystal structure of dengue dimeric iNS1 [10] shows that the crystal packing
262 contains a trimer of dimers (i.e., hexamer) organization; however, there are very few
263 interactions between the three dimers (Fig. 3B(ii)). Their positions in the crystal lattice are
264 mainly supported by their interactions with other iNS1 molecules inside the crystal unit cell.
265 This suggests that the hexameric packing of iNS1 may not be physiological. Comparison of
266 our cryoEM sNS1 hexamer to this crystal hexamer packing shows a very different
267 organization of dimers –they are rotated by ~90° relative to each other (Fig. 3B(i) and (ii),
268 right).

269 It is possible that the loose tetrameric structure is a transition intermediate of the
270 hexameric structure (Fig. 3C). However, we observed loose tetramers forming ~74% of the
271 particle population (Fig. 1D), while hexamers only form ~3%, suggesting that the loose
272 tetramer may be a preferred or a lower energy oligomerization state.

273 It is possible that both the loose tetrameric and the hexameric structures are stabilized
274 by lipids. To test this, we incubated the NS1 sample with detergent (0.05% DDM) and
275 imaged it by cryoEM SPA. We observed that the percentage of loose tetramers and hexamers

276 decreased dramatically after detergent treatment (Extended data Table 2), compared to
277 untreated NS1 (Fig. 1E). This suggests that the lipids inside the loose tetramers and hexamers
278 could be important for their structural integrity. A caveat to this conclusion is the detergent
279 could also disrupt the hydrophobic interactions between the dimers.

280 **CryoEM structure of sNS1 complexed with Fab 5E3**

281 We also investigated the cryoEM structure of sNS1 complexed with the Fab fragment
282 of an anti-NS1 antibody 5E3. The 2D class averages (Fig. 4A) of the boxed particles from the
283 cryoEM micrographs suggest that, when bound by Fabs, most sNS1 particles become dimeric.
284 Unbound stable tetramers were also present (Fig. 4A) and formed ~18% of the total particles.
285 It suggests that the Fab 5E3 can readily dissociate the sNS1 loose tetrameric and hexameric
286 structures. The stable tetrameric structure, on the other hand, is more resistant to Fab binding.

287 The structure of the Fab 5E3:sNS1 dimer complex was determined to an overall
288 resolution of 3.5Å (Fig. 4B, and Extended data 7A), as measured by gold standard FSC curve
289 cutoff at 0.143 (Extended data Fig. 7B). The sNS1 dimer:Fab complex has an overall arch
290 shape, where the Fabs bind to both ends of the β-ladders of the sNS1 dimer (Fig. 4B and
291 Extended data Fig.7A) and are tilted towards the β-roll side of the sNS1.

292 Fab 5E3 interacts with the end of the β-ladder of NS1 (Fig. 4B, Extended data Figs. 7-
293 8) via mainly the Fab heavy chain (Extended data Table 3). The 5E3 epitope is similar to two
294 other previously published Fab:NS1 dimer complex [19,20] – Fabs 2B7 and 1G5.3 (Extended
295 data Fig. 8). Comparison of these structures shows that these three Fabs bind at different
296 angles to the NS1 β-ladder. It has been postulated previously[10] that the hydrophobic β-roll
297 may bind directly to cellular membranes (Extended data Fig. 1), which could be important for
298 its pathogenesis, and therefore the binding orientation of Fab 5E3 may hinder this interaction.
299 A similar neutralization mechanism was suggested for Fab 2B7 [20].

300 We observed that these NS1 dimers have β-roll structures (Figs. 4B and Extended
301 data Fig.7C). This suggests that they are likely not derived from the stable tetramer which has
302 an elongated β-sheet structure. Hence, they could be a broken down product of Fab binding to
303 sNS1 loose tetramers (which contain β-roll structures) and perhaps also the hexamers. We
304 superimposed the Fab:dimer complexes into the loose tetramer and hexamer, and they
305 showed Fabs when bound, could clash with the neighbouring NS1 dimer (Extended data Fig.
306 9A-B). Analysis of the solvent accessibility of the epitopes on the loose tetramer (Extended
307 data Fig. 9C) shows two of the epitopes (orange spheres) are partially exposed (37.5%), while
308 the other two (cyan spheres), are fully exposed. All epitopes in the hexamer (Extended data
309 Fig. 9D) are partially exposed (37.5%). Since Fab likely could bind to the loose tetramer and
310 hexamer. This suggests that the loose tetramers and hexamers likely undergo motions that
311 will at some time point, have their epitopes fully exposed for Fab binding, and once the Fab
312 has bound, the loose tetramer and hexamers could be dismantled into dimers.

313 We reconstructed the unbound stable tetramer to 3.9Å resolution (Fig. 4C (i)), it is
314 identical to the uncomplexed stable tetramer (Fig. 2). Analysis of the epitopes on all NS1
315 molecules in the unbound stable tetramer shows they are only partially exposed (37.5%)
316 (Extended data Fig. 9E), thus discouraging Fab binding. Superposition of the Fab 5E3:dimer
317 complex with one of the dimers in the stable tetramer structure (Fig. 4C (ii)) also shows that
318 the Fab if bound, will clash with the wing domain of the neighbouring dimer. While the Fab
319 is able to cause dissociation between dimers in the loose tetramer and hexamer, it is unable to
320 do the same to the stable tetramer. This suggests that the two dimers in the stable tetramer
321 have tighter interactions, thus disallowing antibody binding. The presence of unbound stable
322 tetramer is consistent with the results of the TEER assay (Fig. 4D), showing Fab can only
323 partially inhibit sNS1 induced endothelial cell hyperpermeability.

In conclusion, since the loose tetramer and hexamers are less stable, their quaternary structure can be easily disrupted by antibody binding. This may form part of the antibody neutralization mechanism. The stable tetramer is however more resistant to Fab 5E3 binding, and this may help sNS1 to evade the host immune response.

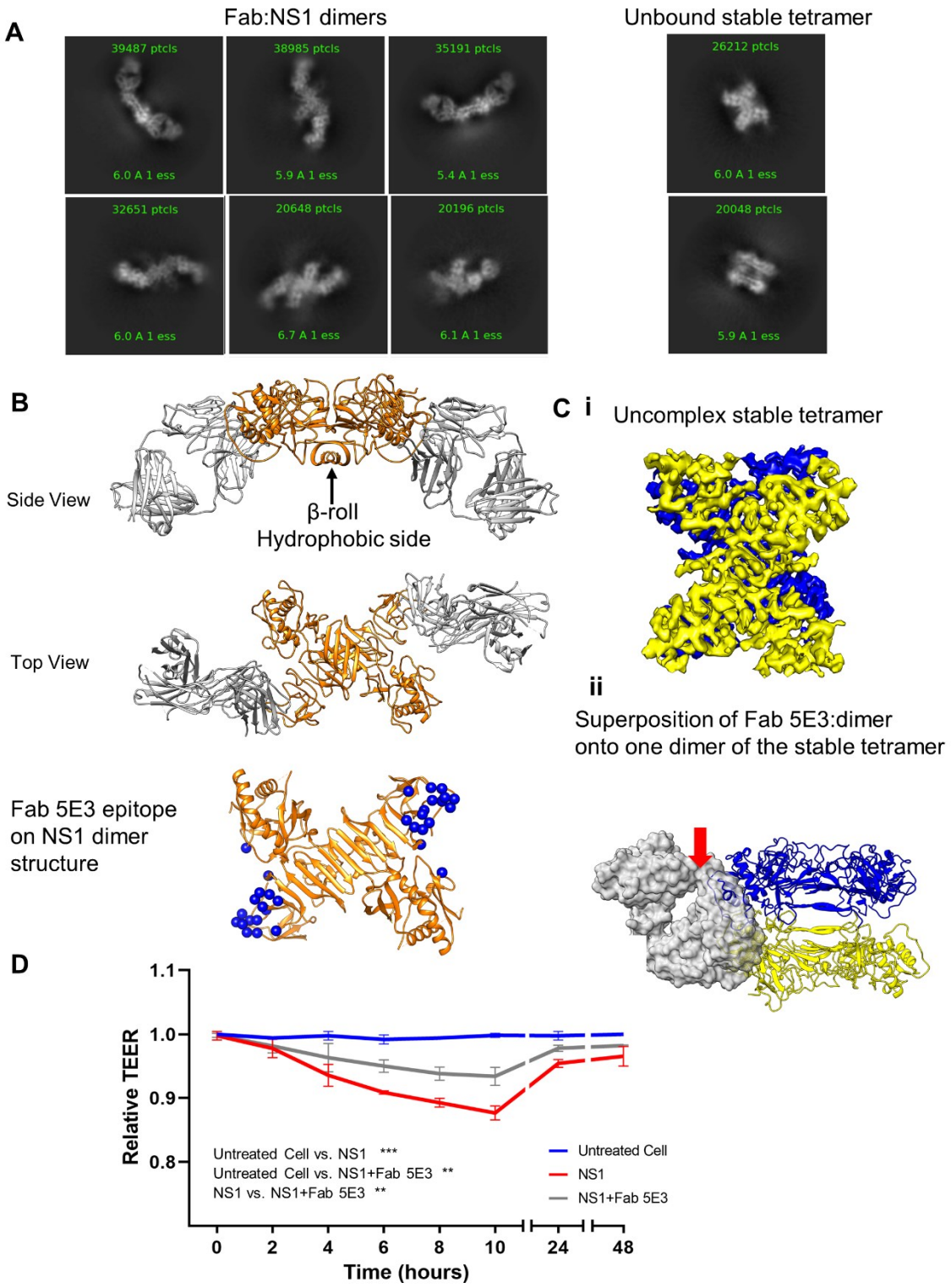

Fig. 4 CryoEM structure of sNS1 complexed with Fab 5E3. **(A)** Some of the 2D class averages showing Fab bound dimers and also unbound stable tetramers. **(B)** The 3.5Å resolution structure of dimer NS1(orange) complexed with Fab 5E3 (grey) shows that they form an arch shape – the Fabs are bending towards the β-roll side of the sNS1 dimer. This NS1 dimer contains the β-roll structure which is also present in the loose tetramer and the

335 hexamer. The Fabs bind to the ends of the β-ladder. The 5E3 epitope is shown as blue
336 spheres. **(C) (i)** The 3.9Å resolution sNS1 unbound tetramer map. The two dimers of the
337 tetramer are colored in blue and yellow. **(ii)** Superposition of Fab 5E3:dimer onto one dimer
338 (yellow) of the stable tetramer shows that Fab (transparent grey surface) when bound will
339 clash (red arrow) with the neighboring dimer (blue). **(D)** TEER assay showing Fab 5E3 can
340 only partially prevent sNS1 from inducing human umbilical vein endothelial cell
341 hyperpermeability. Data are the mean ± SEM from three independent experiments.
342 Statistically significant differences between distinct groups (all time points combined for
343 each group) compared to the untreated groups were determined by a two-way ANOVA
344 analysis using Dunnett's test for multiple comparisons. (***$p < 0.001$ and **$p < 0.01$).

345

346 ## Discussion

347 Previous studies [13,14,21] and our cross-linking experiments of sNS1 (Fig. 1B)
348 consistently showed the presence of dimers, tetramers, and hexamers in semi- and fully
349 denaturing SDS PAGE gel. Syzdykova *et al*. also showed by native gel that yellow fever
350 virus sNS1 consists of mainly tetramers with little hexamers [22]. Our cryoEM study shows the
351 vast majority of sNS1 particles from a DENV2 clinical strain (PVP 94/07) exist as tetramers,
352 while the hexamer only forms a minor population (Fig. 1E). Flamand and colleagues [21]
353 performed small angle X-ray scattering (SAXS) experiments on sNS1 and observed particles
354 with a homogenous gyration radius of 10nm (100 Å), which they concluded were likely
355 hexamers. When we measured the dimensions of our cryoEM sNS1 tetrameric and hexameric
356 structures (Extended data Fig. 3), their longest dimensions are the same (~100 Å), thus
357 correlating well with size of particles detected by the SAXS[21]. This suggests that SAXS may
358 not be able to effectively differentiate between the heterogenous populations of the particles
359 within the sNS1 sample.

360 NS1 plays multiple roles in dengue virus infection of mammalian cells and also
361 mosquitoes. It was shown that sNS1 is one of the major factors contributing to the
362 development of DHF/DSS in patients. Our cryoEM studies show structural details of this
363 important sNS1 protein – (1) the quaternary organization of the different native
364 oligomerization states, (2) how an antibody could bind and dismantle the loose tetrameric and
365 hexameric sNS1 structures and also (3) how sNS1 stable tetramers could resist this antibody-
366 induced disassembly. These findings will contribute to the design of therapeutics and
367 vaccines against severe dengue disease.

368

369

370 **Methods**

371 **sNS1 cloning, expression and purification**

372 DENV 2 PVP94/07 NS1-HisTag was cloned into the pcDNA 3.4-TOPO (Invitrogen) and the
373 plasmid was transfected into Expi293 HEK cells (Thermo Fisher). After expression in HEK
374 cells, we harvested the supernatant containing sNS1. It was then clarified by centrifuging at
375 9000 x g at 4°C for 30 min. The sNS1 protein was purified by using a HisTrap column (GE
376 Healthcare). It was then further purified through a gel-filtration chromatography (Superdex
377 200 10/300 GL column (GE Healthcare)) in buffer (50 mM Tris 8.0 and 150 mM NaCl).
378 Protein purity was then assessed by SDS-PAGE.

379

380 **BS^3 cross-linking of protein**

381 BS^3, a cross-linker with an 11.4 Å spacer arm, were added to NS1 in PBS to a final
382 concentration of 5mM and the samples were incubated for 10, 20, 30 mins at room
383 temperature. Reactions were stopped by adding Tris·HCl, pH 7.5 to a final concentration of
384 50mM and then the sample was added the SDS-PAGE loading buffer, boiled for 2 min and
385 then analyzed on a 4–20 % SDS-PAGE gradient gels (Bio-Rad). The protein bands were then
386 transferred to a nitrocellulose membrane, probed with anti-polyHistidine–peroxidase
387 antibody and visualized by chemiluminescence.

388

389 **CryoEM sample preparation**

390 Quantifoil Au R1.2/1.3 grids were glow-discharged at 5mA for 1min using an Emitech
391 K100X Glow Discharge Unit. About 2.1 µl of sNS1 (0.25 mg/mL) / sNS1 complexed with
392 Fab 5E3 (molar ratio 1:1.2, final concentration of sNS1 is 0.25 mg/mL) were applied to the
393 grids, blotted with a filter paper (Ted Pella Standard Vitrobot filter paper, Grade 595) for 2s
394 (Blot force 2, Blot Time 2 seconds, drain time 0.5 seconds, Humidity 100%) to remove
395 excess sample, and then flash frozen in liquid ethane by using the Vitrobot Mark IV plunger
396 (FEI, Netherlands). To ensure temperature consistency, the temperature of the Vitrobot
397 humidity chamber was adjusted to 4 °C for blotting.

398

399 **CryoEM image acquisition and reconstruction procedure**

400 CryoEM micrographs of sNS1/ sNS1 complex were collected using a Titan Krios
401 transmission electron microscope operated at 300kV and equipped with a Gatan K3 direct
402 electron detector and Gatan GIF post-column energy filter operated in zero-loss mode with a
403 slit width of 20 eV. Images were recorded at a nominal magnification of 130,000.

404 SerialEM was used to carry out the automated data collection. Image shift was used to target
405 9 exposures per stage position with an image shift of 1.6 um. Images were recorded by movie
406 mode, with similar total exposure of 4.9s, 58 frames per movie and total dose of 81.5 e-/Å2.
407 The frames from each movie were aligned using MotionCor2 [23] to produce full dose images
408 used for particle selection and orientation search. The images were taken at underfocus in the
409 0.8-2.0 µm range. In total, 7714 micrographs were collected for the sNS1. The astigmatic

410 CTF parameters were estimated with Patch CTF estimation in CryoSPARC [16] and were
411 accounted for during orientation search. We performed automated particle picking using
412 Warp [24] and CryoSPARC. A total of 2,342,754 particles were selected. These particles were
413 binned 4x before going through 20 iterations of 2D classification (CryoSPARC) to produce
414 2D class averages. The starting model was generated by the CryoSPARC Ab-Initio
415 Reconstruction. We then performed 25 iterations of 3D classification and reconstruction
416 using C1 symmetry using the program Relion [15] to remove broken and distorted particles. We
417 then switched to CryoSPARC to perform further 3D classification. For the class with stable
418 tetramers, we performed multiple cycles of heterogenous and non-uniform refinement [16] by
419 imposing D2 symmetry. For the loose tetramers, we performed heterogenous, non-uniform
420 refinement without any symmetry imposed. We then performed local refinement on one of its
421 dimers. For the hexamers, we performed only non-uniform refinement with D3 symmetry
422 imposed. The cryoEM reconstruction flow chart is summarized in Extended data Fig. 2.
423 Resolution was determined by using gold standard Fourier shell correlation and local map
424 resolution was estimated with ResMap [25]. The refinement statistics are shown in Extended
425 data Table 1.

426

427 **Protein structure building**

428 The sNS1 structures were first interpreted by approximate fitting using the ZIKA NS1 dimer
429 structure (PDB 5GS6) as rigid bodies into the density using "fit-in-map" function in Chimera
430 [18]. We then used COOT to mutate the residues to those of dengue virus NS1 sequence and
431 then fit individual residues into densities [26]. We then refined the structures using the
432 "phenix.real_space_refine" procedure in the Phenix software package, with default
433 parameters and rigid body refinement using secondary-structure and torsion angle restraints [27].
434 The final coordinates containing an asymmetric unit (i.e., a protomer in the stable tetramer
435 structure) were then used to build the biological unit (full tetramer) by using the command
436 "sym" in UCSF Chimera [18]. The final coordinates of the asymmetric units were checked
437 using MolProbity [28]. Maps and structures shown in the Figs were generated by using UCSF
438 Chimera and Coot.

439

440 **TEER assay**

441 A monolayer of Human Umbilical Vein endothelial cells (80%–90% confluency) cultured in
442 T75 flasks were detached using trypsin-EDTA (0.25%). The cells were then resuspended
443 using fresh culture media and then counted using an automated cell counter. 60,000 cells (300
444 µL per well) were seeded onto the apical side of Transwell inserts. Each Transwell was
445 transferred inside a 24-well format plate containing 1.5 mL of endothelial cell culture media.
446 Transwells containing endothelial cells were incubated at 37°C and 5% CO2 for 3~4 days,
447 and 50% of the culture medium was changed in each well 48 hours post-seeding. Cells were
448 grown until the TEER values reached ~ 160 to 170 Ohms (Ω), indicating 100% cell
449 confluency. After this, 3 µg NS1 protein / NS1_Fab5E3 complex (molar ratio 1:1.2) was
450 added to the apical side of the Transwell insert. Electrical resistance values, measured in
451 Ohms (Ω), were recorded at every 2-hour time-points following the addition of the proteins
452 using an Epithelial Volt Ohm Meter with the "chopstick" electrodes. Endothelial permeability

was expressed as relative TEER which represents a ratio of resistance values (Ω) as follows: (Ω experimental condition - Ω medium alone)/(Ω nontreated endothelial cells - Ω medium alone).

Data availability

The cryoEM map and the atomic models of the all sNS1 and sNS1:Fab structures have been deposited in the Electron Microscopy Data Bank and the Protein Data Bank - stable tetramer (EMD: 32841, PDB: 7WUT), loose tetramer (EMD: 32842 and PDB: 7WUU), Dimer of Loose tetramer (EMD: 32840 and PDB: 7WUS), hexamer (EMD: 32842 and PDB: 7WUV) and sNS1:Fab5E3(EMD: 32839 and PDB: 7WUR).

References

1 Gubler, D. J. Dengue and dengue hemorrhagic fever. *Clin Microbiol Rev* **11**, 480-496, doi:10.1128/CMR.11.3.480 (1998).

2 Thomas, S. J. & Yoon, I. K. A review of Dengvaxia(R): development to deployment. *Hum Vaccin Immunother* **15**, 2295-2314, doi:10.1080/21645515.2019.1658503 (2019).

3 Halstead, S. B. Neutralization and antibody-dependent enhancement of dengue viruses. *Adv Virus Res* **60**, 421-467, doi:10.1016/s0065-3527(03)60011-4 (2003).

4 Beatty, P. R. *et al.* Dengue virus NS1 triggers endothelial permeability and vascular leak that is prevented by NS1 vaccination. *Sci Transl Med* **7**, 304ra141, doi:10.1126/scitranslmed.aaa3787 (2015).

5 Carpio, K. L. & Barrett, A. D. T. Flavivirus NS1 and Its Potential in Vaccine Development. *Vaccines (Basel)* **9**, doi:10.3390/vaccines9060622 (2021).

6 Modhiran, N. *et al.* Dengue virus NS1 protein activates immune cells via TLR4 but not TLR2 or TLR6. *Immunol Cell Biol* **95**, 491-495, doi:10.1038/icb.2017.5 (2017).

7 Puerta-Guardo, H., Glasner, D. R. & Harris, E. Dengue Virus NS1 Disrupts the Endothelial Glycocalyx, Leading to Hyperpermeability. *PLoS Pathog* **12**, e1005738, doi:10.1371/journal.ppat.1005738 (2016).

8 Libraty, D. H. *et al.* High circulating levels of the dengue virus nonstructural protein NS1 early in dengue illness correlate with the development of dengue hemorrhagic fever. *J Infect Dis* **186**, 1165-1168, doi:10.1086/343813 (2002).

9 Liu, J. *et al.* Flavivirus NS1 protein in infected host sera enhances viral acquisition by mosquitoes. *Nat Microbiol* **1**, 16087, doi:10.1038/nmicrobiol.2016.87 (2016).

10 Akey, D. L. *et al.* Flavivirus NS1 structures reveal surfaces for associations with membranes and the immune system. *Science* **343**, 881-885, doi:10.1126/science.1247749 (2014).

11 Xu, X. *et al.* Contribution of intertwined loop to membrane association revealed by Zika virus full-length NS1 structure. *EMBO J* **35**, 2170-2178, doi:10.15252/embj.201695290 (2016).

12 Wang, D. *et al.* A Mutation Identified in Neonatal Microcephaly Destabilizes Zika Virus NS1 Assembly in Vitro. *Sci Rep* **7**, 42580, doi:10.1038/srep42580 (2017).

13 Muller, D. A. *et al.* Structure of the dengue virus glycoprotein non-structural protein 1 by electron microscopy and single-particle analysis. *J Gen Virol* **93**, 771-779, doi:10.1099/vir.0.039321-0 (2012).
14 Gutsche, I. *et al.* Secreted dengue virus nonstructural protein NS1 is an atypical barrel-shaped high-density lipoprotein. *Proc Natl Acad Sci U S A* **108**, 8003-8008, doi:10.1073/pnas.1017338108 (2011).
15 Scheres, S. H. RELION: implementation of a Bayesian approach to cryo-EM structure determination. *J Struct Biol* **180**, 519-530, doi:10.1016/j.jsb.2012.09.006 (2012).
16 Punjani, A., Rubinstein, J. L., Fleet, D. J. & Brubaker, M. A. cryoSPARC: algorithms for rapid unsupervised cryo-EM structure determination. *Nat Methods* **14**, 290-296, doi:10.1038/nmeth.4169 (2017).
17 Punjani, A., Zhang, H. & Fleet, D. J. Non-uniform refinement: adaptive regularization improves single-particle cryo-EM reconstruction. *Nat Methods* **17**, 1214-1221, doi:10.1038/s41592-020-00990-8 (2020).
18 Pettersen, E. F. *et al.* UCSF Chimera--a visualization system for exploratory research and analysis. *J Comput Chem* **25**, 1605-1612, doi:10.1002/jcc.20084 (2004).
19 Modhiran, N. *et al.* A broadly protective antibody that targets the flavivirus NS1 protein. *Science* **371**, 190-194, doi:10.1126/science.abb9425 (2021).
20 Biering, S. B. *et al.* Structural basis for antibody inhibition of flavivirus NS1-triggered endothelial dysfunction. *Science* **371**, 194-200, doi:10.1126/science.abc0476 (2021).
21 Flamand, M. *et al.* Dengue virus type 1 nonstructural glycoprotein NS1 is secreted from mammalian cells as a soluble hexamer in a glycosylation-dependent fashion. *J Virol* **73**, 6104-6110, doi:10.1128/JVI.73.7.6104-6110.1999 (1999).
22 Syzdykova, L. R. *et al.* Fluorescent tagging the NS1 protein in yellow fever virus: Replication-capable viruses which produce the secretory GFP-NS1 fusion protein. *Virus Res* **294**, 198291, doi:10.1016/j.virusres.2020.198291 (2021).
23 Zheng, S. Q. *et al.* MotionCor2: anisotropic correction of beam-induced motion for improved cryo-electron microscopy. *Nat Methods* **14**, 331-332, doi:10.1038/nmeth.4193 (2017).
24 Tegunov, D. & Cramer, P. Real-time cryo-electron microscopy data preprocessing with Warp. *Nat Methods* **16**, 1146-1152, doi:10.1038/s41592-019-0580-y (2019).
25 Kucukelbir, A., Sigworth, F. J. & Tagare, H. D. Quantifying the local resolution of cryo-EM density maps. *Nat Methods* **11**, 63-65, doi:10.1038/nmeth.2727 (2014).
26 Emsley, P. & Cowtan, K. Coot: model-building tools for molecular graphics. *Acta Crystallogr D Biol Crystallogr* **60**, 2126-2132, doi:10.1107/S0907444904019158 (2004).
27 Adams, P. D. *et al.* PHENIX: a comprehensive Python-based system for macromolecular structure solution. *Acta Crystallogr D Biol Crystallogr* **66**, 213-221, doi:10.1107/S0907444909052925 (2010).
28 Williams, C. J. *et al.* MolProbity: More and better reference data for improved all-atom structure validation. *Protein Sci* **27**, 293-315, doi:10.1002/pro.3330 (2018).

Acknowledgments

We thank Valerie S-Y Chew, Xinni Lim and Qunfei Zhou for help in experiments. This work was supported by Duke-NUS Signature Research Programme funded by the Ministry of Health, Singapore and National Research Foundation Investigatorship award (NRF-NRFI2016-01) awarded to SML. AWKT is supported by a Khoo Postdoctoral Fellowship Award (Duke-NUS-KPFA/2021/0044) from Duke-NUS Medical School and the Estate of Tan Sri Khoo Teck Puat.

Author information

Affiliations

Program in Emerging Infectious Diseases, Duke-National University of Singapore Medical School, Singapore 169857, Singapore.

Bo Shu, Justin S.G. Ooi, Aaron W.K Tan, Thiam-Seng Ng, Guntur Fibriansah, Victor A. Kostyuchenko, Shee-Mei Lok

Centre for Bio-Imaging Sciences, Department of Biological Sciences, National University of Singapore, Singapore 117557, Singapore.

Bo Shu, Aaron W.K Tan, Thiam-Seng Ng, Guntur Fibriansah, Victor A. Kostyuchenko, Shee-Mei Lok

Center for Bioimaging Sciences, National University of Singapore, Singapore, 117557, Singapore.

Jian Shi, Shee-Mei Lok

Medical Sciences Division, University of Oxford, Oxford OX3 9D

Wanwisa Dejnirattisai, Juthathip Mongkolsapaya, Gavin Screaton

Contributions

S.M.L. supervised the project. S.M.L. and B.S. designed research studies; J.S.G.O. produced sNS1. W.D., J.M. and G.S. produced Fab. B.S. and J.S.G.O. conducted experiments. T.S.N., A.W.K.T. and J.S. collected cryo-EM data; S.M.L., B.S., G.F. and V.A.K. analyzed data; S.M.L. and B.S. wrote the manuscript.

Corresponding author

Correspondence to Shee-Mei Lok.

Ethics declarations

Competing interests

The authors declare no competing interests.

Additional information

Extended Data Fig. 1

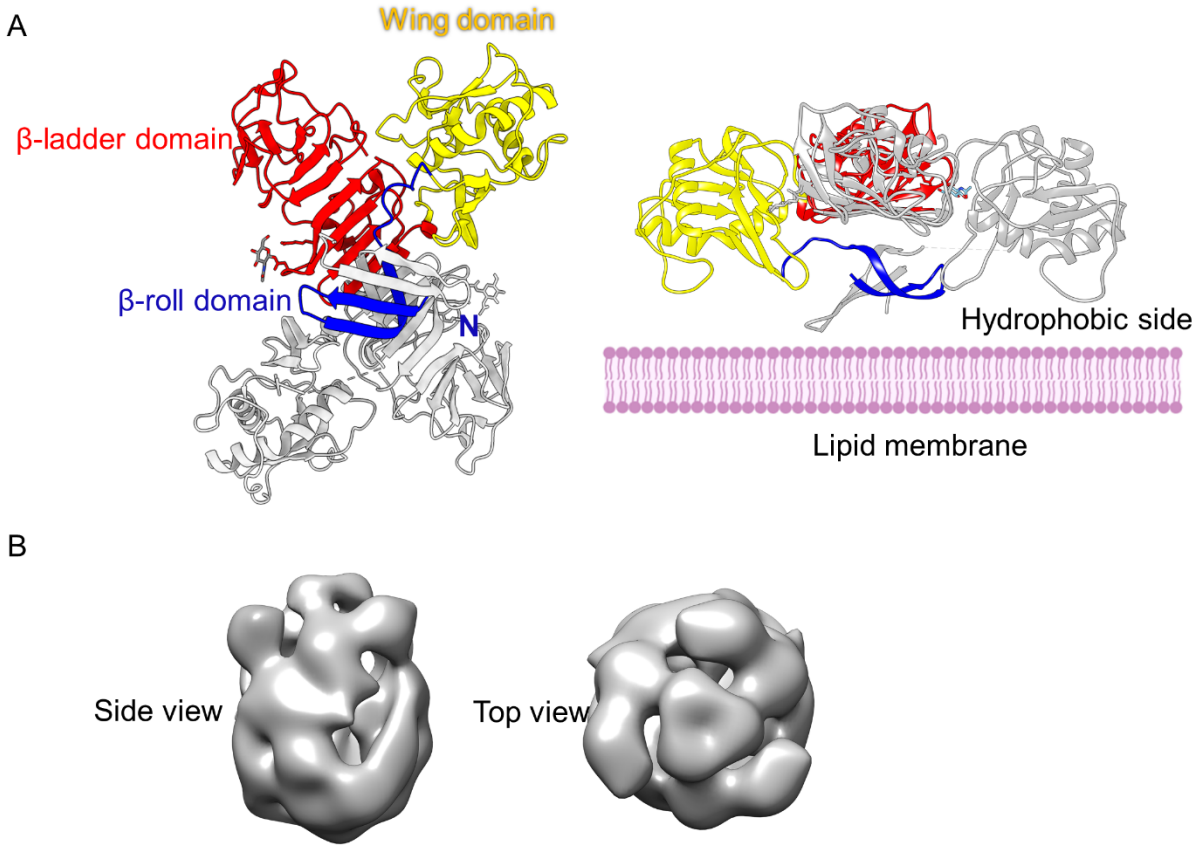

Extended Data Fig. 1 Previously published structures of the dengue NS1. (A) Crystal structure of dengue dimeric iNS1 (PDB:5GS6). Left: top view, looking from the β-roll of the iNS1 dimer. One protomer contains three domains: starting from the N-terminus- β-roll (blue), wing domain (yellow) and the β-ladder (red). It interacts with the other protomer (colored in grey) through extensive hydrogen bonds. Right: side view of the iNS1 dimer. The β-roll is highly hydrophobic and is predicted to interact with the cellular membrane. (B) A previously published low resolution EM reconstruction of the sNS1 (EMDB:2073). This map is reconstructed from negatively stained sNS1 and C3 symmetry was imposed [13].

590 **Extended Data Fig. 2**

591

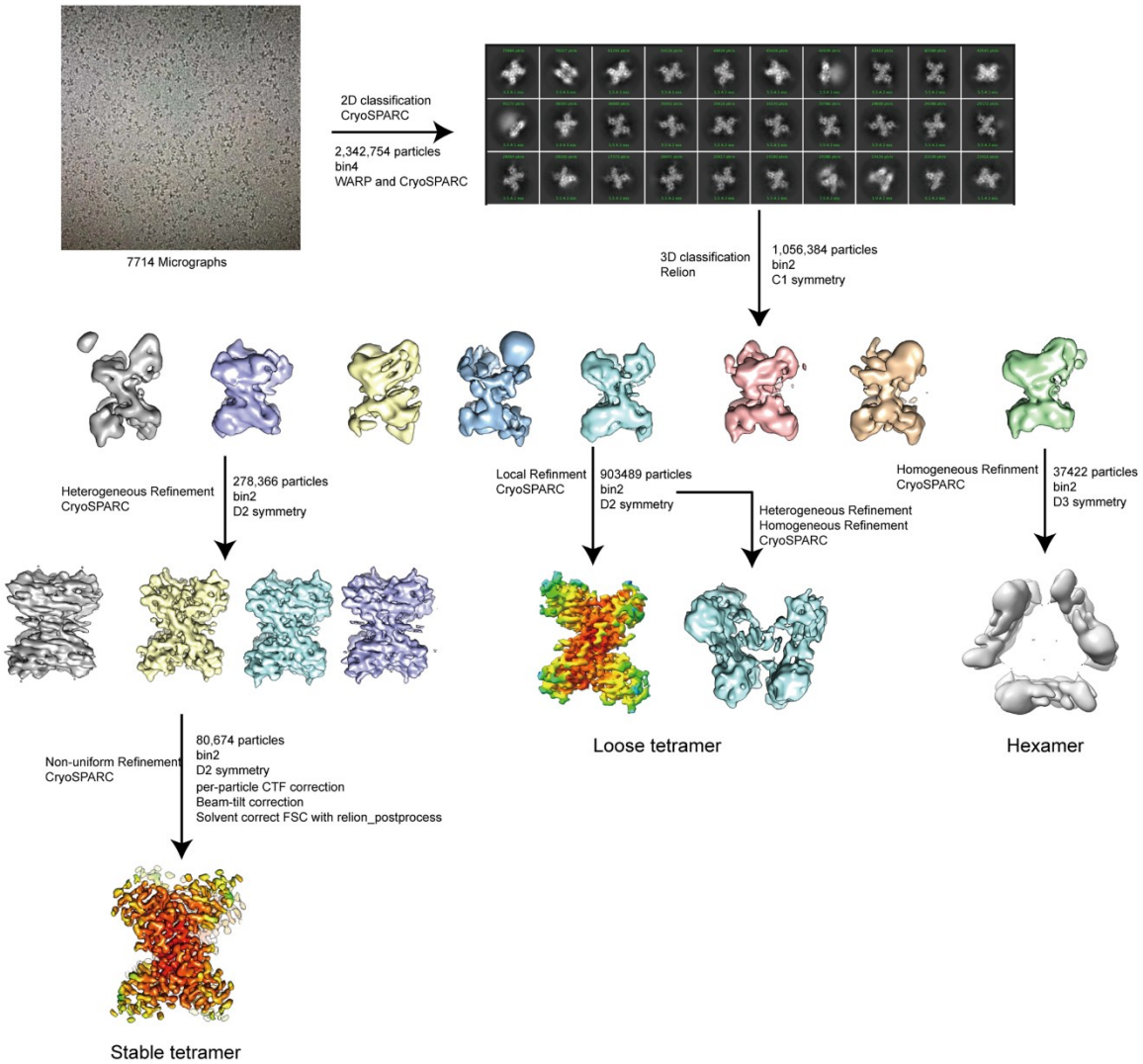

592

593 **Extended Data Fig. 2 The cryoEM reconstruction workflow for uncomplexed sNS1.**

594

595

596 **Extended Data Fig. 3**

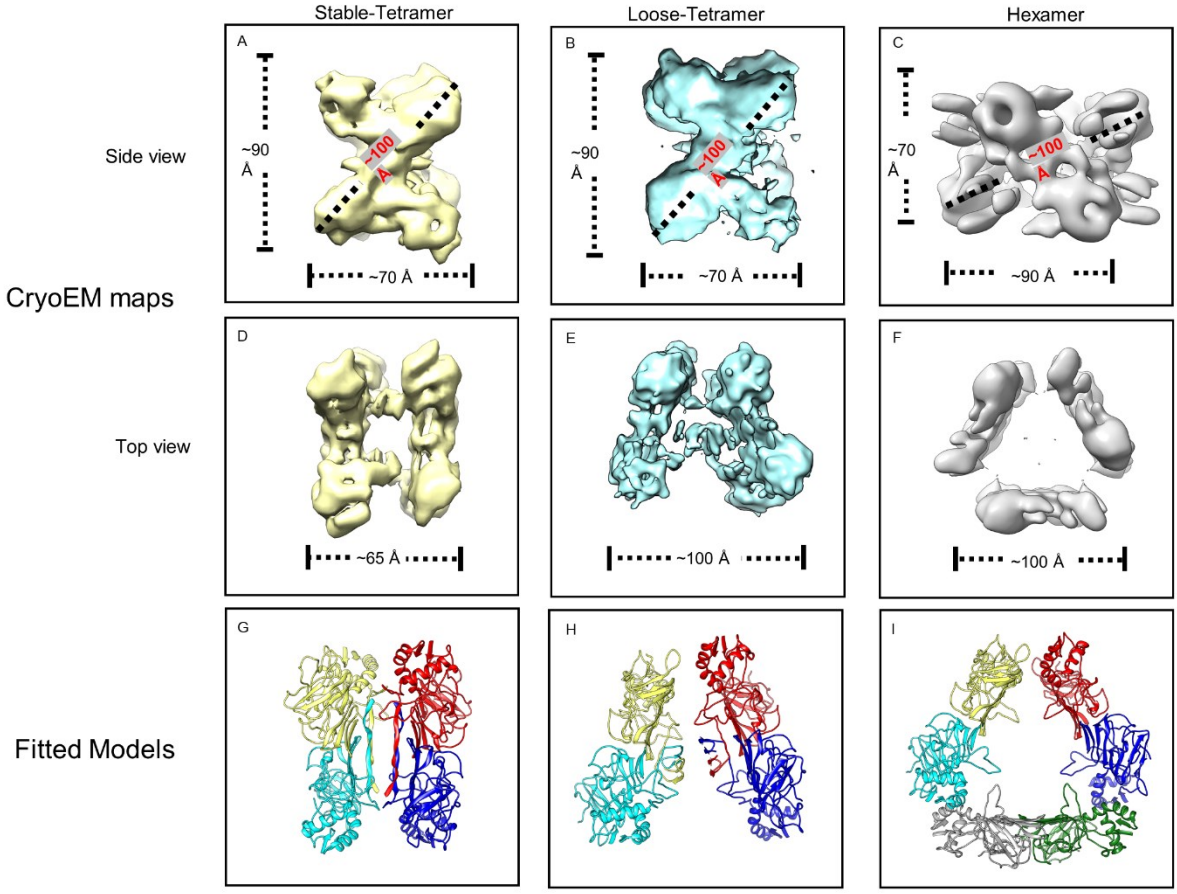

597

598 **Extended Data Fig. 3 The initial sNS1 cryoEM maps after 3D classification using C1**
599 **symmetry.** Dimensions of the stable, loose tetramers and hexamers are shown. Fitted models
600 are shown on the bottom row.

601

602 **Extended Data Fig. 4**

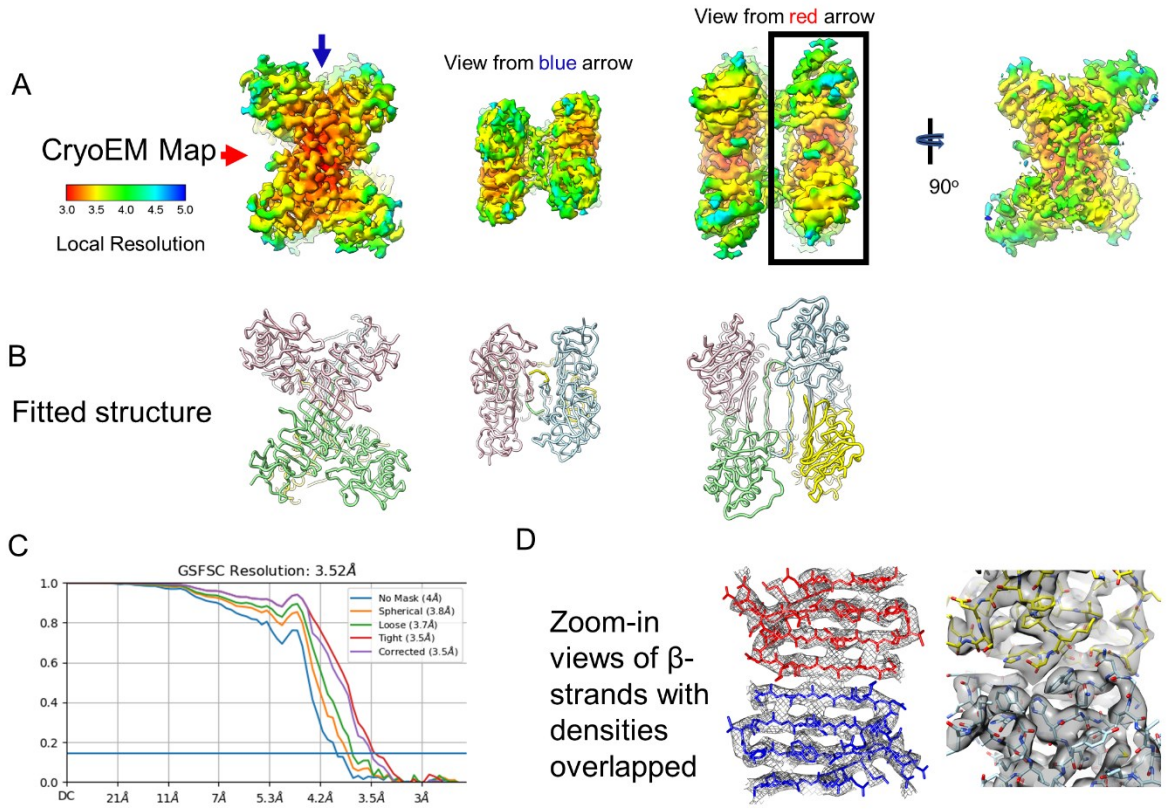

603

604 **Extended Data Fig. 4 The 3.5Å resolution sNS1 stable tetrameric structure.** (A) Different
605 views of the cryoEM map displayed at high contour level. The densities are colored
606 according to their local resolution. (B) The fitted structure show in the same view as the
607 cryoEM map directly above (in (A)). There are two dimers facing each other. One dimer is
608 colored in pink and green, while the other is light blue and yellow. (C) Fourier shell
609 correlation plot showing resolution. (D) Zoom-in views of density map showing the β-strands
610 densities are well resolved (left). Some of the side chains densities (right) can also be
611 observed.

612

613

614

615 **Extended Data Fig. 5**

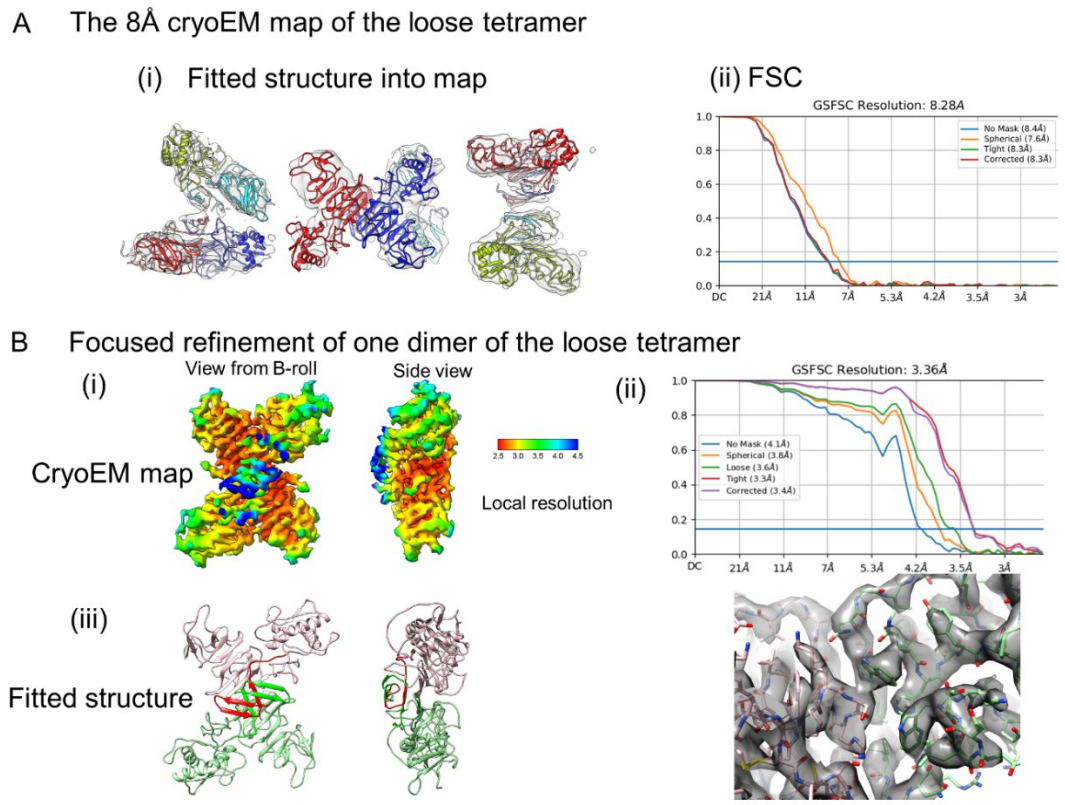

616

617 **Extended Data Fig. 5 CryoEM maps of the sNS1 loose tetramer.** (A) 8Å cryoEM map of the loose
618 tetramer. (i) Different views of the fitted structure of the loose tetramer into the density map
619 (transparent grey). (ii) FSC plot showing resolution. (B) The 3.4Å cryoEM map of one dimer of the
620 loose tetramer after focused refinement. (i) Different views of the cryoEM map. Density is colored
621 according to local resolution. (ii) Up: FSC plot showing resolution of the map: Down: zoom-in view
622 showing that some side chain densities are well resolved. (iii) The fitted structure of one of the dimers
623 (pink and light green) is very similar to that of dengue iNS1. The β-roll in each protomer is colored in
624 a darker shade of the respective protomer's color.

625 **Extended Data Fig. 6**

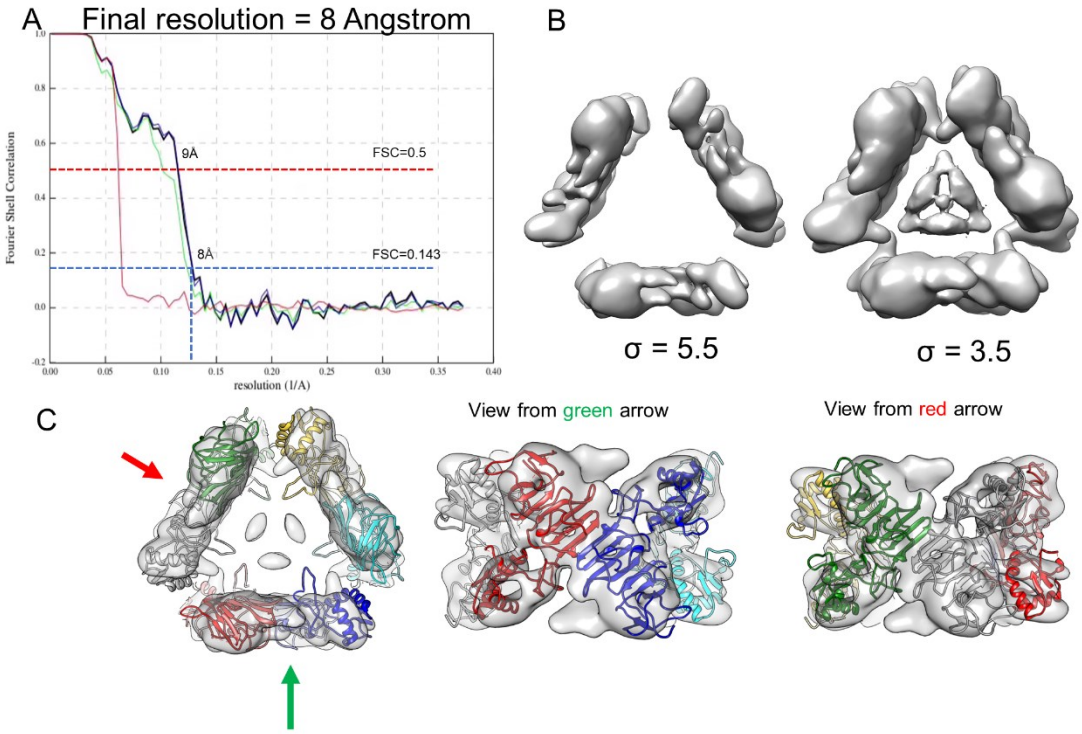

626

627 **Extended Data Fig. 6 The 8Å cryoEM map of the sNS1 hexamer.** (A) FSC plot showing
628 resolution of the map. (B) The hexamer density displayed at different contour levels. At lower
629 contour levels, densities at the interior of the hexamer can be seen. (C) Different views of the
630 fit of the three dimers into the hexamer density map.

631

632 **Extended Data Fig. 7**

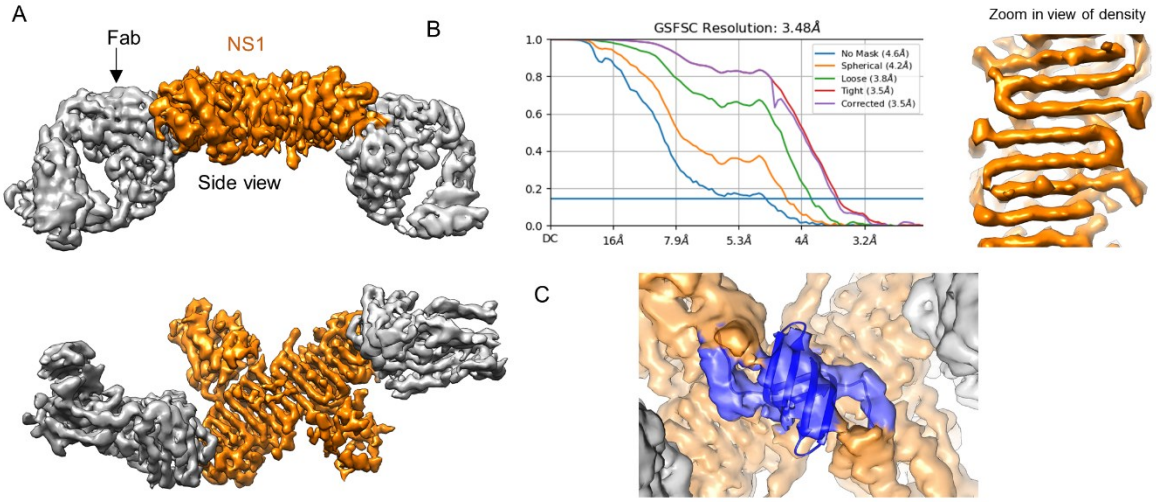

633

634 **Extended Data Fig. 7 3.5Å resolution cryoEM structure of Fab 5E3:sNS1 dimer.** (A)
635 Side and top views of the cryoEM map of the Fab 5E3:sNS1 dimer. NS1 is colored in orange
636 while Fabs in grey. (B) Left: FSC plot showing the resolution of the map. Right: zoom-in
637 view showing well-resolved β-strands. (C) Zoom-in view of the fitted β-roll into its
638 corresponding density.

639

640

641 **Extended Data Fig. 8**

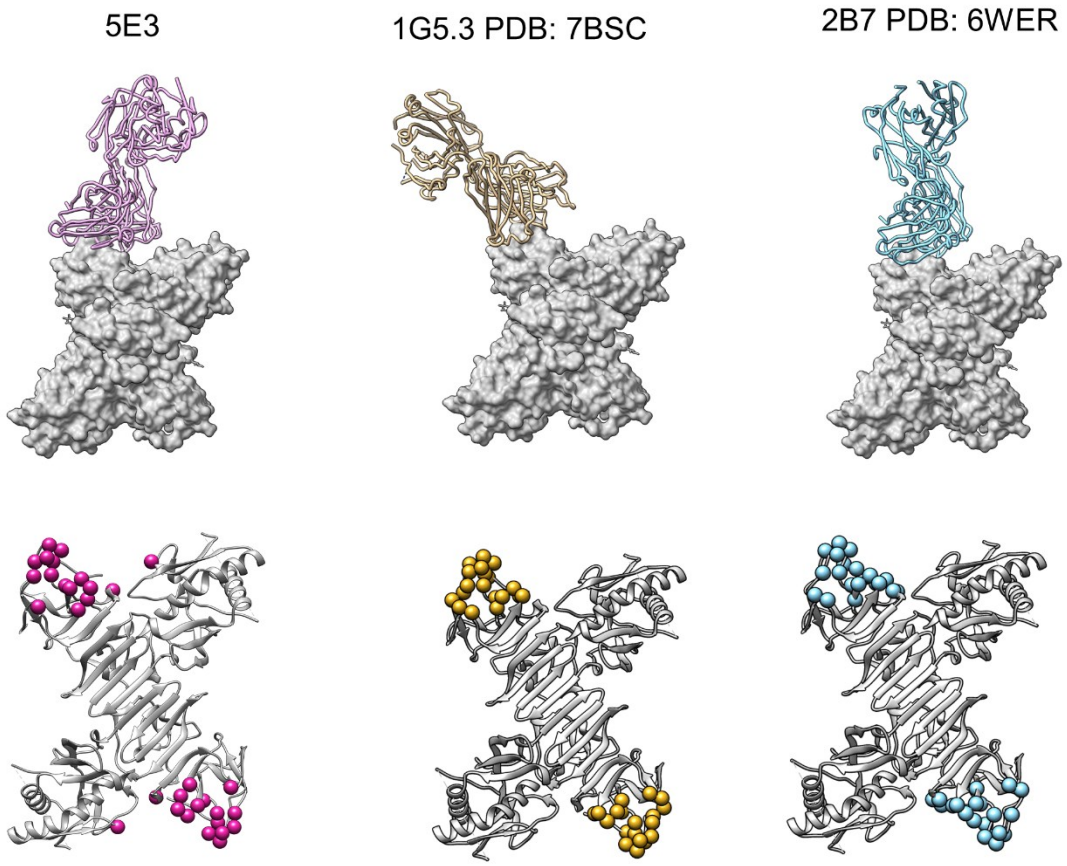

642

643

644 **Extended Data Fig. 8 Comparison of the binding (top panels) and epitope (bottom**
645 **panels) of Fab 5E3 to other previously published Fab:NS1 complexes [19,20].**

646

647

648 **Extended Data Fig. 9**

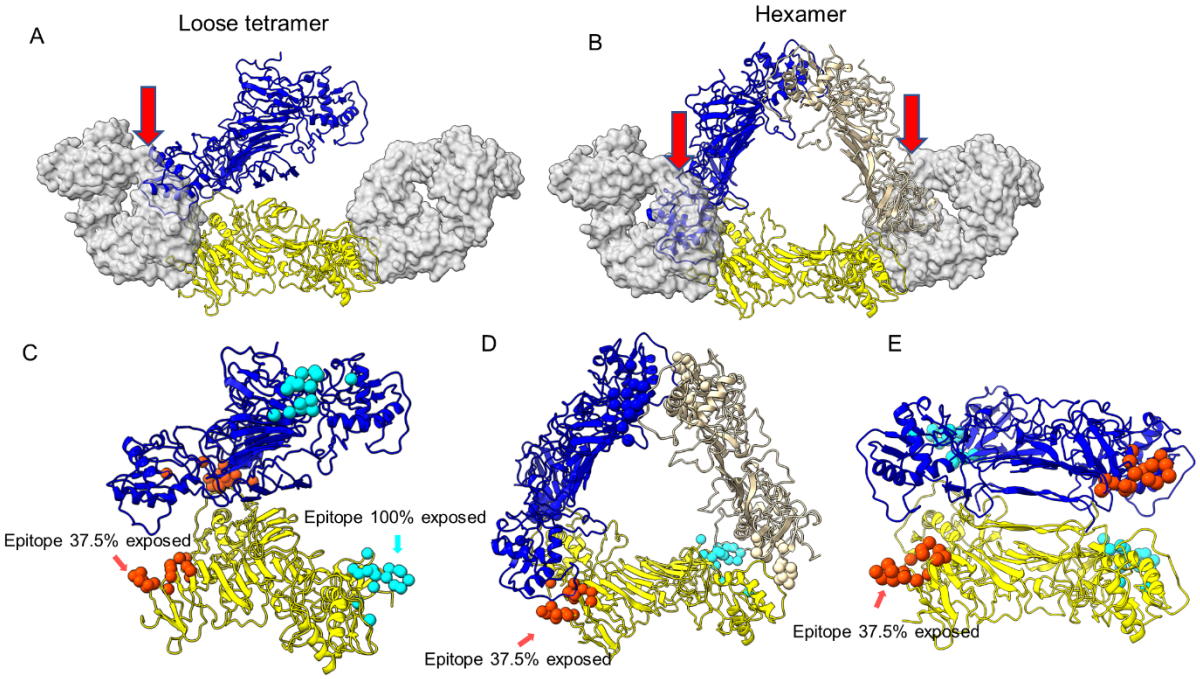

649

650 **Extended Data Fig. 9** Superposition of Fab 5E3:dimer into the (A) loose tetramer and (B)
651 hexamer and the analysis of percentage exposure of epitopes (C-E) in the stable, loose
652 tetramers and hexamers. (A-B) Superposition of Fab 5E3:dimer onto one dimer (yellow) of
653 the loose tetramer and hexamer. Fab is shown as transparent grey surface and clashes with
654 neighboribg NS1 dimer is indicated with red arrows. (C-E) The percentage exposure of
655 epitopes in the oligomers. The two epitopes within one dimer are colored in orange and cyan.
656 (C) In the loose tetramer, 37.5% of the orange epitope is exposed while the cyan epitope is
657 fully exposed (100%). (D) In the hexamer, 37.5% of both the orange and cyan epitopes are
658 exposed. (E) In the stable tetramer, the two epitopes are both 37.5% exposed.

659

660

	DENV2_NS1_Tetramer	DENV2_NS1_dimer	DENV_NS1_Fab5E3
Data collection and processing	(EMDB-32841) (PDB 7WUT)	(EMDB-32840) (PDB 7WUS)	(EMDB-32839) (PDB 7WUR)
Microscope	FEI Titan Krios	FEI Titan Krios	FEI Titan Krios
Camera	Gatan K3	Gatan K3	Gatan K3
Magnification	130,000 ×	130,000 ×	130,000 ×
Voltage (kV)	300	300	300
Electron exposure (e^- /$Å^2$)	81.5	81.5	80.1
Defocus range (μm)	-0.8 to -2.0	-0.8 to -2.0	-0.8 to -2.0
Exposure rate (e^- /A^2/sec)	8.74	8.86	8.35
Number of frames per movie	58	58	58
Pixel size (Å)	0.66	0.66	0.66
Energy filter slit width (eV)	20	20	20
Automation software	SerialEM	SerialEM	SerialEM
Symmetry imposed	D2	C1	C1
Micrographs used	7714	7714	7145
Total number of extracted particles	2,342,754	2,342,754	1,264968
Total number of refined particles	278,366	454,477	273,074
Number of particles in final map	80,674	181,587	95,895
Map resolution (Å)	3.5	3.3	3.5
FSC threshold	0.143	0.143	0.143
Refinement			
Initial model used (PDB code)	5GS6	5GS6	5GS6
Refinement package, (resolution cutoff)	Phenix, real-space refinement (3.5)	Phenix, real-space refinement (3.3)	Phenix, real-space refinement (3.5)

Resolution of unmasked and masked reconstructions at 0.5 and 0.143 FSC	Unmasked 3.3/3.9 Masked 3.3/3.8	Unmasked 3.5/4.0 Masked 3.5/3.9	Unmasked 3.5/4.1 Masked 3.4/3.9
Map sharpening *B* factor (Å^2)	-230	-210	-105.9
Model composition			
Non-hydrogen atoms	11,176	5,456	8,928
Protein residues	1400	682	1134
Ligands	0	0	0
Global CC (CCvol)	0.88	0.85	0.79
Local CC (CCmask)	0.77	0.84	0.78
B factors (Å^2)			
Protein	88.90	93.61	134.83
Ligand	-	-	-
R.m.s. deviations			
Bond lengths (Å)	0.009	0.005	0.009
Bond angles (°)	1.116	1.042	1.000
Validation			
MolProbity score	2.70	2.35	2.49
Clashscore	31.67	18.75	24.01
Poor rotamers (%)	0.00	0.00	0.00
C-beta deviations	0.00	0.00	0.00
Ramachandran plot			
Favored (%)	81.54	88.94	87.25
Allowed (%)	18.46	11.06	12.75
Disallowed (%)	0	0	0
CaBLAM outliers (%)	8.89	6.08	5.05

EMRinger score	2.70	2.26	2.65

Extended Data Table 1 Cryo-EM data collection, refinement and validation statistics

	Stable Tetramer	Loose Tetramer	Hexamer
Particles	126130	90928	0
Percentage	58%	42%	0 %

Extended Data Table 2 The percentage of particles in different oligomerization states determined after 3D classification of NS1 treated with detergent (0.05% DDM).

NS1	Fab Heavy Chain	Fab Light Chain
138		27(CDR1)
269		94(CDR3)
281	52/53/54/55/56(CDR2)	
299	102/103(CDR3)	
301	33(CDR1)	
302	103(CDR3)	
303	103(CDR3)	
304	32/106(CDR1/CDR3)	
305	31/33/103(CDR1/CDR3)	
306	31(CDR1)	
307	31/53(CDR1/CDR2)	
324	56(CDR2)	
325	57(CDR2)	
326	57/102/100(CDR2/CDR3)	
327	100/102(CDR3)	94(CDR3)
328	100(CDR3)	

Extended Data Table S3 List of hydrogen bonds/electrostatic interactions between Fab 5E3 (heavy and light chains) with the NS1 protein. The interacting CDRs of the Fabs are indicated.